Journal of Microwaves, Optoelectronics and Electromagnetic Applications, Vol. 21, No. 3, September 2022
DOI: http://dx.doi.org/10.1590/2179-10742022v21i3261941

Optimization Techniques and Mathematical Modeling Applied to Reluctance Motors

B. B. Miranda[1], J. A. Malagoli[2], J. R. Camacho[1],
[1]*Postgraduate Program in Electrical Engineering, FEELT, Universidade Federal de Uberlândia, Uberlândia MG, Brazil, brenobm@ufu.br, jrcamacho@ufu.br*
[2]*Postgraduate Program in Electrical Engineering, PPGEE, Universidade Federal do Paraná, Curitiba PR, Brazil, juliana.malagoli@ufpr.br*

***Abstract*– The present work aims at the application of different optimization strategies in the electromagnetic analysis of the Variable Reluctance Motor (VRM) through Finite Element (FE) simulation. Two case studies are investigated: the first one aims to optimize the geometry and electrical characteristics of windings of a single-phase VRM 6/6, minimizing copper losses; the second aims to optimize a restricted set of geometric parameters of a 4-phase VRM 8/6, maximizing the flux linkage in the phase coils per unit volume of magnetic core. In this way, by using the Finite Element Method (FEM), the results from the Differential Evolution (DE) and Particle Swarm Optimization (PSO) algorithms will be compared and highlighted. Then, the magnetic flux densities of the motors are analyzed before and after the optimization. The results obtained show good efficiency of the algorithms, since the objective functions were satisfied with respect to the reference models.**

Index Terms– Differential Evolution, Finite Element Method, Optimization Techniques, Particle Swarm Optimization, Variable Reluctance Motor.

I. INTRODUCTION

Variable reluctance machines can either act as a motor or generator, have variable speed, are low-cost, and can provide high efficiency at the medium and high-speed range. This type of machine has aroused the interest of several researchers in recent years, making it a strong competitor compared with other electric machines on the market [1].

One of the most notable features of the Variable Reluctance Motor (VRM) is the abscense of coils in the rotor, in addition to being more suitable to running at high-speed and high-temperature conditions. This implies that all winding resistive losses occur in the stator. Often the stator can be cooled more efficiently than the rotor, resulting in a smaller motor for a given power and size specification [2], [3].

With the technological development of digital systems and power electronic devices, the difficulties inherent in the complexity of control began to be overcome, making VRM competitive when compared with the other types of most commonly used machines. The construction of a VRM drive is not straightforward since the power semiconductors have to be selected according to the motor ratings [4]. Therefore, defining the motor ratings is an issue addressed to the design stage. In order to proper control a VRM at low- and high-speed, the electric and magnetic parameters must be determined.

In this way, two problems arise:

- Knowledge of motor parameters;
- Identify suitable commutation angles.

Brazilian Microwave and Optoelectronics Society-SBMO *received 12 Mar 2022; for review 20 Mar 2022; accepted 2 July 2022*
Brazilian Society of Electromagnetism-SBMag *ISSN 2179-1074*

The Finite Element Method (FEM) has become popular, among other well-established techniques, for numerically solving differential equations that arise in mathematical engineering and modeling. It is a powerful method for multi-physics analysis, so optimizations will become more important by relating overall performance and total manufacturing costs, thus, analyses of coupled problems are of increasing interest. Hence, the first mentioned problem can be addressed to the Finite Element Analysis (FEA). The second problem can be solved by developing look-up tables, which describe the relationship between flux linkage and current excitation over rotor position.

The main contributions, justifications, advantages and impacts of this work are:

- Show the implementation of two different units: the first case is a virtual motor model, designed by using an analytical project calculation method only for optimization purposes; the second case is a prototype model designed, built and mounted in an induction motor housing for experimental study.
- The prototype motor was presented as the second case in order to evaluate the possible performance improvement through the geometric dimensions optimization for further feasibility study concerning the prototyping of the enhanced model.
- Design and optimize variable reluctance motors, aiming to improve performance and efficiency, due to the increasing demands of rational use of energy and greater competitiveness of industries;
- Use open source computational tools to simulate fine prototypes through FEA by exploring the motor symmetry in order to reduce the computational time;
- Compare the results of designed electrical machines before and after optimization with real motors data using the Differential Evolution (DE) and Particle Swarm Optimization (PSO) algorithms;
- Assemble prototypes before the construction of a machine, leading to reduce manufacturing costs and minimize environmental impacts on the production of motors applied to electric vehicles, for example.

The solution for optimization problems aiming to improve a model consists in the use of smart algorithms, such as the DE and the PSO algorithms. The DE algorithm is a powerful global optimizer known for its reliable results and fast convergence [5], whereas the PSO technique was successful applied in many single-objective optimization problems [6]. Therefore, the algorithms were chosen for carrying out the single-objective optimization problems; the classic DE version was used for the former. Among various multi-objective evolutionary algorithms, the Speed-constrained Multi-objective PSO (SMPSO) was chosen to be applied into a bi-objective problem, rather than the very famous Non-dominated Sorting Genetic Algorithm II (NSGA-II), for instance. These choices were led by the great performance of the algorithms. In the work [7], the SMPSO has reached the best values for three quality indicators in eigth (average) out of twelve problems, when compared with five state-of-the-art multi-objective optimization algorithms (two genetic algorithms, a scatter search, a cellular genetic algorithm and a bio-inspired PSO version).

The focus of this article is to investigate and compare optimization techniques for minimizing and maximizing objective functions by using open source finite element solvers. In this context, computational tools such as FEMM (Finite Element Method Magnetics) software are used to generate magnetic flux density results and compute copper losses in the single-phase VRM 6/6, and ONELAB (Open Numerical Engineering LABoratory) software to calculate the flux linkage and generate magnetic flux densities in a 4-phase 8/6 VRM.

Brazilian Microwave and Optoelectronics Society-SBMO *received 12 Mar 2022; for review 20 Mar 2022; accepted 2 July 2022*
Brazilian Society of Electromagnetism-SBMag *ISSN 2179-1074*

II. RELUCTANCE MOTORS

Variable reluctance motors (VRMs) have a simple, low-cost and robust construction, mounted from a compact rotor and stator with non-oriented grain steel laminations and concentrated windings at stator poles. This work aims to perform studies of a single-phase variable reluctance motor 6/6 and a four-phase 8/6 motor in order to verify operational aspects and, particularly, the efficiency of these machines. In summary, some of its main characteristics are: high robustness, fault tolerance, high starting conjugate, operating capacity as motor or generator and absence of coils or permanent magnets in the rotor. Such characteristics make VRM a machine for aerospace applications, where robustness and tolerance to faults are important, and electrical traction, where fault tolerance is imperative and the ability to operate as a generator can be used for regenerative braking, for example [8], [9].

A. The 6/6 VRM Design

In general, machine designs start from the desired output power for the system. In this way, this principle will be used in the single-phase variable reluctance motor. Fig. 1 shows the dimensions that must be calculated for a single-phase VRM design.

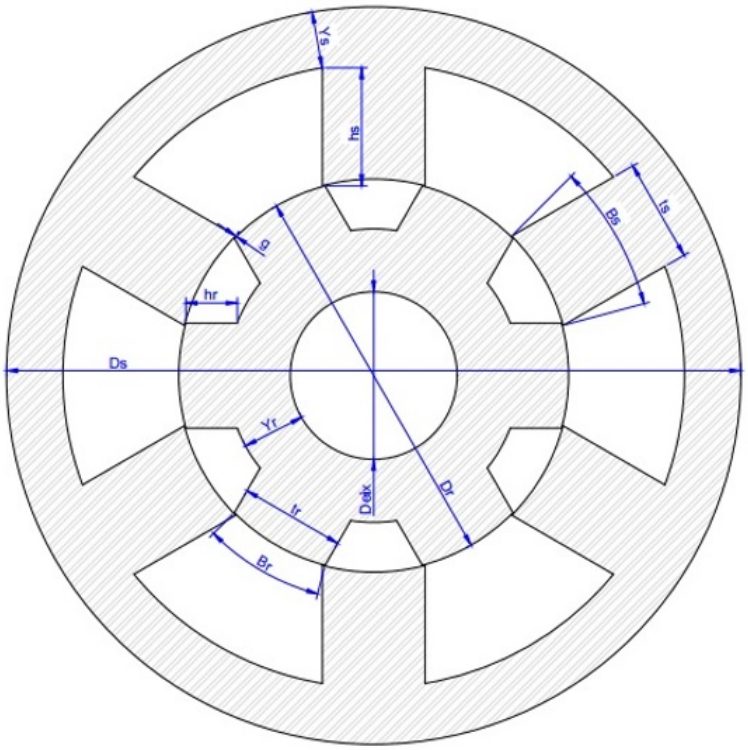

Fig. 1. Dimensions of the Single-Phase Variable Reluctance Motor.

Where $Deix$ is the diameter of the central axis (mm); Dr is the rotor diameter (mm); Ds is the stator diameter (mm); tr is the rotor pole width (mm); ts is the stator pole width (mm); βr is the rotor polar arc (degrees); βs is the stator polar arc (degrees); hs is the height of the stator pole (mm); hr is the height of the rotor pole (mm); Ys is the width of the stator yoke (mm); Yr is the width of the rotor yoke (mm); g is the airgap length (mm). The output power is given by [10].

$$P = \frac{TRV.k1.\omega.\pi.Dr}{4}. \tag{1}$$

Brazilian Microwave and Optoelectronics Society-SBMO *received 12 Mar 2022; for review 20 Mar 2022; accepted 2 July 2022*
Brazilian Society of Electromagnetism-SBMag *ISSN 2179-1074*

Where TRV being the set by rotor volume; $k1$ is the constant of the relationship between the rotor diameter and the length of a machine; ω is the conversion from revolutions per minute (rpm) to radians per second.

Some works in the variable reluctance motor design literature [10]–[12] state that the ratio of rotor diameter to stator external diameter should vary between 0.4 and 0.7. Furthermore, the minimum value for the stator and rotor arc is given by (2).

$$min(\beta s, \beta r) = \frac{4\pi}{Ns.Nr}. \tag{2}$$

Where Ns is the number of stator poles; Nr is the number of rotor poles. In Fig. 1, the stator yoke (Ys) is shown, where it must support half of the flux that passes through the poles, which is given by (3).

$$Ys = 1.1\left[\left(\frac{Dr}{2} + g\right) sin\left(\frac{\beta s}{2}\right)\right]. \tag{3}$$

Where g is the air gap (mm), that is, the distance between the stator and the rotor plates. It is observed that the value of the air gap must be close to 0.5% of the rotor diameter to minimize the reluctance when aligned [10], [12].

The widths and heights of the stator and rotor poles, respectively, can be calculated by (4), (5), (6) and (7).

$$ts = 2\left[\left(\frac{Dr}{2} + g\right) sin\left(\frac{\beta s}{2}\right)\right]. \tag{4}$$

$$hs = \left(\frac{Ds - Dr}{2}\right) - g - Ys. \tag{5}$$

$$tr = ts + 2g. \tag{6}$$

$$hr = \frac{ts}{2}. \tag{7}$$

According to [13], the rotor yoke height, Yr, should be calculated by half the rotor pole width, tr. It must insert an increase of 20% to 40%, in the case, 20% is used to keep the dimensions reduced.

Sizing the coils is done in two steps: first the number of turns of each coil is calculated and then the coil conductor is determined. As shown by [11]:

$$NE = \frac{2g}{Ip}\frac{Bent}{\mu_0}. \tag{8}$$

$$ac = \frac{Ip}{Jc\sqrt{q}}. \tag{9}$$

Where NE is the number of turns; Ip is the peak value of phase current (A); $Bent$ is the magnetic flux density in the airgap (T); ac is the conductor cross-sectional area (mm^2); q is the number of phases; Jc is the current density (A/mm^2); μ_0 is the vacuum magnetic permeability ($4\pi.10^{-7}$ H/m).

At steady-state, Ip is related to the maximum allowable value reached after the current rise time when the phase is fed by a converter. In addition, (9) defines the current density as the ratio of rms value of the current over the conductor cross-sectional area.

received 12 Mar 2022; for review 20 Mar 2022; accepted 2 July 2022

ISSN 2179-1074

B. The 8/6 VRM Design

Based on the design procedure presented in the previous section and following the output power principle, a 4-phase 8/6 VRM with a rated power of 2.2 kW was developed in [14]. The motor is designed for insertion in a 100L model frame.

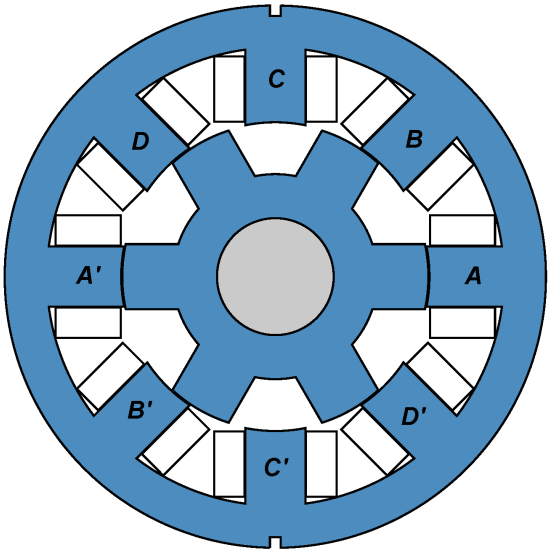

Fig. 2. Design of the 4-Phase 8/6 Variable Reluctance Motor.

Fig. 2 shows the 8/6 VRM model with the four phase windings, A-A', B-B', C-C' and D-D', in which each pair of coils are connected in series. The same dimensions defined for the 6/6 VRM are also valid here.

III. Optimization Techniques

After the design stage of a VRM, pole arc angles and the other dimensions should be optimized through optimization techniques in order to satisfy some performance requirements. In this section, two single-objective and one multi-objective optimization algorithms are presented: a differential evolution algorithm, DE, a particle swarm optimization, PSO, and the PSO-based, SMPSO.

A. Differential Evolution

The differential evolution algorithm was developed for optimization problems [15]. The choice of the DE algorithm is based on the following characteristics:

- It is a stochastic search algorithm, originated from natural selection;
- The algorithm seeks the global optimal solution by manipulating a population of solutions;
- It is effective for solving discontinuous objective function optimization problems, as it does not require information about its derivatives;
- Input and output parameters are handled like real ordinary numbers with no extra processing;
- It presents a purely mathematical concept, based on vector operations, and for this reason it is considered a structural approach.

Fig. 3 shows a flowchart of the differential evolution algorithm. The main idea of DE is to generate new individuals, with emphasis on modified vectors or donors, by adding the weighted difference vector

received 12 Mar 2022; for review 20 Mar 2022; accepted 2 July 2022

ISSN 2179-1074

between two random individuals from the population to a third individual, whose operation is called mutation [5].

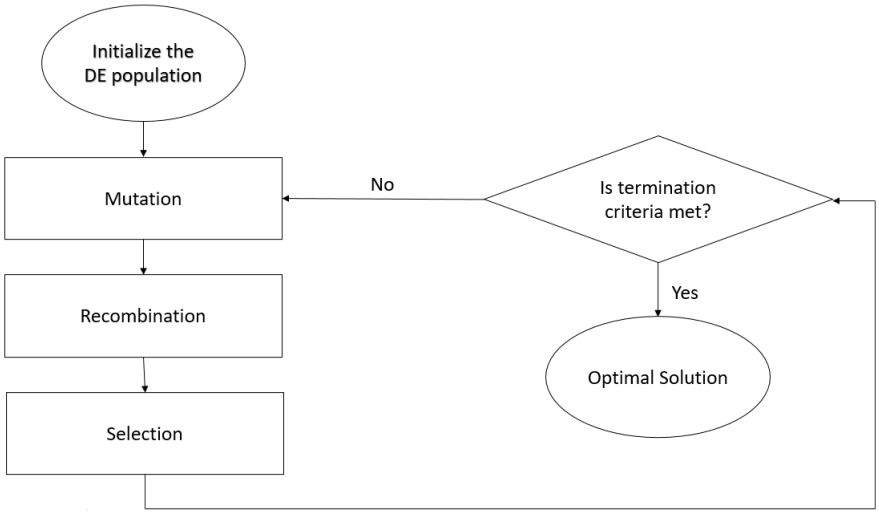

Fig. 3. Flowchart of DE algorithm.

The components of the new donor individual are mixed with the components of the randomly chosen individual, to result in the so-called tentative vector, or experimental vector. The process of mixing parameters is called crossover by the evolutionary algorithm's community. As third individual is randomly chosen, this method refers to the classic DE version that uses uniform crossover (DE/rand/1/bin), where the term "rand" indicates that the base vector is randomly chosen; the term "1" means that only one vector difference is used to form the mutated population and the term "bin" indicates that uniform crossover is employed during the formation of the trial population [5]. If the cost of the experimental vector is less than the cost of the target vector, then the experimental vector will be the target vector of the next generation. This last operation is called selection. The procedure is terminated through some stopping criterion, that is, the maximum number of generations predefined by the user is reached [15].

B. Particle Swarm Optimization

The PSO is a search algorithm based on the simulation of the social behavior of birds in a flock, having been successfully applied in single-objective optimization problems [6]. In the basic swarm strategy for optimization, the population of potential solutions to the problem is called a swarm, whose individuals, or particles, move within the search space. Changes in the position $\vec{x}_i(t)$ of each p_i particle in generation t are based on the tendency of individuals to imitate the success of others. The position is updated according to (10),

$$\vec{x}_i(t) = \vec{x}_i(t-1) + \vec{v}_i(t), \tag{10}$$

and according to the speed $\vec{v}_i(t)$ given by [7],

$$\vec{v}_i(t) = w\vec{v}_i(t-1) + C_1 r_1(\vec{x}_{p_i} - \vec{x}_i) + C_2 r_2(\vec{x}_{g_i} - \vec{x}_i). \tag{11}$$

Where: $\vec{x}_{p_i}$ is the best single solution seen, $\vec{x}_{g_i}$ is the position of the best particle in the entire swarm,

received 12 Mar 2022; for review 20 Mar 2022; accepted 2 July 2022

ISSN 2179-1074

referred to as the leader, w is the particle's inertia coefficient, r_1 and r_2 are random values uniformly distributed over the interval [0, 1], and C_1 and C_2 are learning factors.

C. Speed-constrained Multi-objective PSO

In order to handle multiple objectives and extend the PSO to multi-objective optimization, most PSO-based approaches, generically called Multiple-Objective Particle Swarm Optimizers (MOPSOs), mainly modify the selection process of the particles related to $\vec{x}_{p_i}$ and $\vec{x}_{g_i}$ in the basic PSO algorithm. Moreover, among different MOPSOs, the representative OMOPSO algorithm [6] is based on Pareto dominance and the use of a crowding distance of the NSGA-II for leader selection. This approach avoids choosing any non-dominated solution as a new leader, and with each generation the set of leaders is updated with the best solutions.

In a performance analysis study [7], six representative MOPSO algorithms (including the OMOPSO) were unable to solve some multi-modal problems satisfactorily, pointing out an issue related to the velocity of the particles in these algorithms, which can become too high, resulting in erratic movements. In this sense, the SMPSO algorithm was developed, based on OMOPSO, with the objective of preventing such behavior through a velocity constriction mechanism. The particle's velocity is controlled according to a constriction coefficient instead of using upper and lower values parameter which limit the step size of velocity. Besides, the velocity of the particles are calculated according to (11), and the resulting velocity is then multiplied by the constriction factor [7], which is given by,

$$\chi = \frac{2}{2 - \varphi - \sqrt{\varphi^2 - 4\varphi}} \tag{12}$$

Where φ is closely related to learning factors C_1 and C_2. Therefore, the resulting value is constrained by a mechanism that limits the speed through pre-defined upper and lower parameters. Moreover, in SMPSO a polynomial mutation is applied to the 15% of the particles.

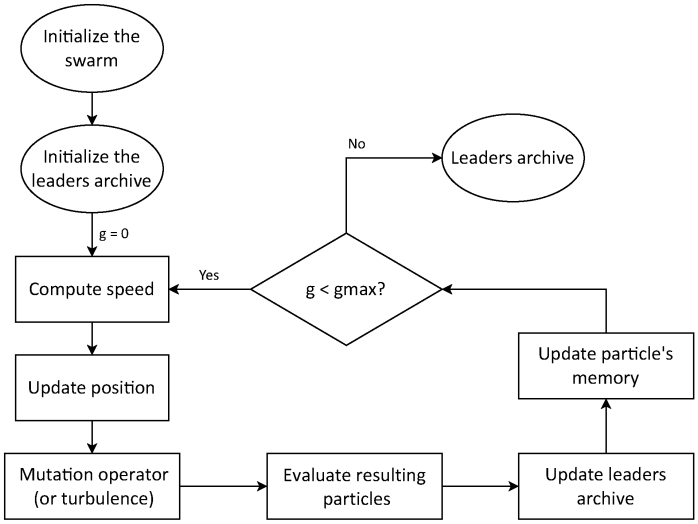

Fig. 4. Flowchart of SMPSO algorithm.

Fig. 4 shows the flowchart of the SMPSO algorithm. The swarm, including the position, velocity and individual best of the particles, and the leaders archive are initialized. The main objective is to update

received 12 Mar 2022; for review 20 Mar 2022; accepted 2 July 2022

ISSN 2179-1074

the positions of the particles based on the calculated velocities and to apply the turbulence operator to accelerate the convergence of the swarm. A set of leaders, in which the maximum size is fixed equal to the size of the swarm, is updated after each iteration (generation). As the leaders archive become full, the crowding distance of NSGA-II is used to filter out leader solutions [7].

IV. Finite Element Method

The Finite Element Method (FEM) emerged during the 1950s for application in aeronautics, becoming an efficient and flexible tool for problems of distribution of electric and magnetic fields [16]–[18]. In addition, it obeys second-order partial differential equations, whose analytical modelling is difficult to solve. Currently, FEM is often used in engineering, so a new project can be improved, designed and optimized computationally, without the construction of numerous prototypes.

The following will be the Maxwell equations, interface conditions, boundary conditions and discretization.

A. Maxwell's Equations

Taking together, the following Maxwell's equations in $\mathbb{R}^3$, considering a quasi-static approximation,

$$\nabla \times \vec{H} = \vec{J} \tag{13}$$

$$\nabla \cdot \vec{B} = 0 \tag{14}$$

and the constitutive relation,

$$\vec{B} = \mu \vec{H} \tag{15}$$

they form a mathematical representation of the magnetostatic problem. Where: $\vec{H}$ is the magnetic field (A/m), $\vec{J}$ is the imposed current density (A/m^2), $\vec{B}$ is the magnetic induction (T) and μ is the magnetic permeability (H/m) [17]. When the magnetic induction is expressed in terms of the magnetic vector potential ($\vec{B} = \nabla \times \vec{A}$), (13)-(15) leads to the magnetostatic formulation used to describe the VRM models,

$$\nabla \times (\nu \nabla \times \vec{A}) = \vec{J} \tag{16}$$

Where ν is the magnetic reluctivity. For considering material nonlinearities, ν is obtained through the relation (15) by providing the nonlinear *B-H* curve from the magnetic material datasheet.

B. Interface Conditions

The Interface Conditions (ICs) determine how the fields are transmitted between an interface, i.e., the ICs represent the coupling of fields between subdomains [17], [18]. Let Σ be the intersection of the subdomains Ω_1 and Ω_2, $\hat{n}$ is the normal unit vector to the surface pointing from Ω_2 and Ω_1, Fig. 5.

received 12 Mar 2022; for review 20 Mar 2022; accepted 2 July 2022

ISSN 2179-1074

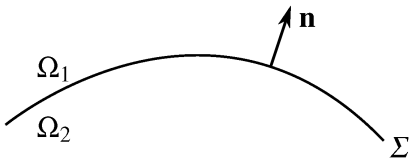

Fig. 5. Surface Σ between the two continuous medium, Ω_1 and Ω_2.

The transmission conditions for the fields $\vec{B}$ and $\vec{H}$ are obtained from the magnetic Gauss law and Ampère law, respectively,

$$\hat{n} \cdot (\vec{B_2} - \vec{B_1})\big|_{\Sigma} = 0 \tag{17}$$

$$\hat{n} \times (\vec{H_2} - \vec{H_1})\big|_{\Sigma} = \vec{J} \tag{18}$$

Where $\vec{B_1}$ and $\vec{H_1}$ are the vector fields located in the medium Ω_1, both assumed to be pointed outward to the surface Σ; $\vec{B_2}$ and $\vec{H_2}$ are the vector fields in the medium Ω_2, both pointing inward to the surface. Equation (17) implies that normal components of the magnetic induction must be continuous through the interface, whereas (18) implies that tangential components of the magnetic field are discontinuous if a current density is imposed on interface.

C. Boundary Conditions

Boundary conditions are constraints imposed on local fields on the boundary of a domain [18]. Let Γ_H and Γ_E be the complementary parts of the boundary Γ of the domain Ω where homogeneous boundary conditions are specified,

$$\hat{n} \times \vec{H}\big|_{\Gamma_H} = 0 \tag{19}$$

$$\hat{n} \cdot \vec{B}\big|_{\Gamma_E} = 0 \tag{20}$$

These conditions can be applied, for instance, on the outer diameter of the VRM shown in Fig. 1, for containing the magnetic field inside the motor.

D. Discretization

Using the weighted residual approach in (16), the partial differential equation is weighted by test functions $\vec{A}'$ over the domain Ω, as follows

$$\int_{\Omega} \nabla \times (\nu \nabla \times \vec{A}) \cdot \vec{A}' d\Omega = \int_{\Omega} \vec{J} \cdot \vec{A}' d\Omega \tag{21}$$

By applying the vector identity $\vec{u} \cdot (\nabla \times \vec{v}) = \nabla \cdot (\vec{v} \times \vec{u}) + \vec{v} \cdot \nabla \times \vec{u}$ in (21), the following so-called weak formulation are obtained,

$$\int_{\Gamma_H} \hat{n} \times \vec{H} \cdot \vec{A}' d\Gamma_H + \int_{\Omega} (\nu \nabla \times \vec{A}) \cdot \nabla \times \vec{A}' d\Omega = \int_{\Omega} \vec{J} \cdot \vec{A}' d\Omega \tag{22}$$

In general, the integral over Γ_H is null due to the test function, thereby the integral is defined as a Dirichlet constraint (19). The finite element method consists in approximating the solution $\vec{A}$ by $\vec{A}_h$

Brazilian Microwave and Optoelectronics Society-SBMO *received 12 Mar 2022; for review 20 Mar 2022; accepted 2 July 2022*
Brazilian Society of Electromagnetism-SBMag *ISSN 2179-1074*

in a finite dimensional domain, in which the subscript *h* indicates the geometric entity length. For first order triangular elements, $\vec{A}_h$ and the test functions are taken in a function space,

$$F^1(\Omega) = span\{\vec{w}_1, \vec{w}_2, \dots \vec{w}_E\} \tag{23}$$

Where: the basis functions $\vec{w}_e, e = 1, \dots, E$ are associated with the *E* edges of the mesh over the domain Ω. Therefore, $\vec{A} \approx \vec{A}_h$ are interpolated by,

$$\vec{A}_h = \sum_{e=1}^{E} u_e \vec{w}_e \tag{24}$$

Where: u_e are the degrees of freedom (or unknowns) associated with circulations of $\vec{A}$ along edges of mesh. Inserting (24) in the weak form (22) and taking for $\vec{A}'$: $\vec{w}_e, e = 1, \dots, E$, the Galerkin method leads to a system of linear equations, for $s = 1, \dots, E$,

$$\sum_{e=1}^{E} u_e \int_{\Omega} (\nu \nabla \times \vec{w}_e) \cdot \nabla \times \vec{w}_s d\Omega = \int_{\Omega} \vec{J} \cdot \vec{w}_s d\Omega \tag{25}$$

or, $[A_{es}][u_e] = [f_s]$ in matrix form. As both machines are composed of saturable materials, the matrix $\mathbf{A}$ depends on the unknown field $\mathbf{u}$, and the system of equations are solved iteratively by means of Newton-Raphson method.

V. CASE STUDIES

The electrical characteristics, the dimensions before optimization, the objective functions and the bounds of the geometric variables of the 6/6 and 8/6 VRMs will be presented. For the optimization procedure in the first case study (6/6 VRM), the FEA is preceded by the analytical procedure, mentioned in the Section II, provided that both electrical and geometric parameters are to be optimized (i.e., equations (1)-(9) must be satisfied). In constrast, for the second case (8/6 VRM), the optimizing parameters are directly modified into FEA.

A. Minimization of Copper Losses in 6/6 VRM

The present case study aims to simulate through the FEMM software the copper losses of the windings and generate the graphs of the magnetic flux density in the motor air gap. In addition, copper losses were minimized via the DE algorithm. To improve the understanding of the methodology proposed in this work, Fig. 6 shows the flowchart with all the stages of this case development. Table I presents the electrical variables of the 6-pole single-phase motor, based on models from a manufacturer.

First, it is calculated from (1) the value of the inner diameter, and then it is possible to calculate the other dimensions. A value greater than that calculated was adopted as a safety margin. Table II shows the calculated dimensions for the motor.

The determination of the conductor cross-section is made by approximating the calculated area with the existing conductors, so it is possible to notice that the most appropriate is the 12 AWG conductor with an area of 3.31 mm^2. Additionally, the steel sheets are M22 non-oriented grain silicon steel that begin to saturate at approximately 1.85 T.

received 12 Mar 2022; for review 20 Mar 2022; accepted 2 July 2022

ISSN 2179-1074

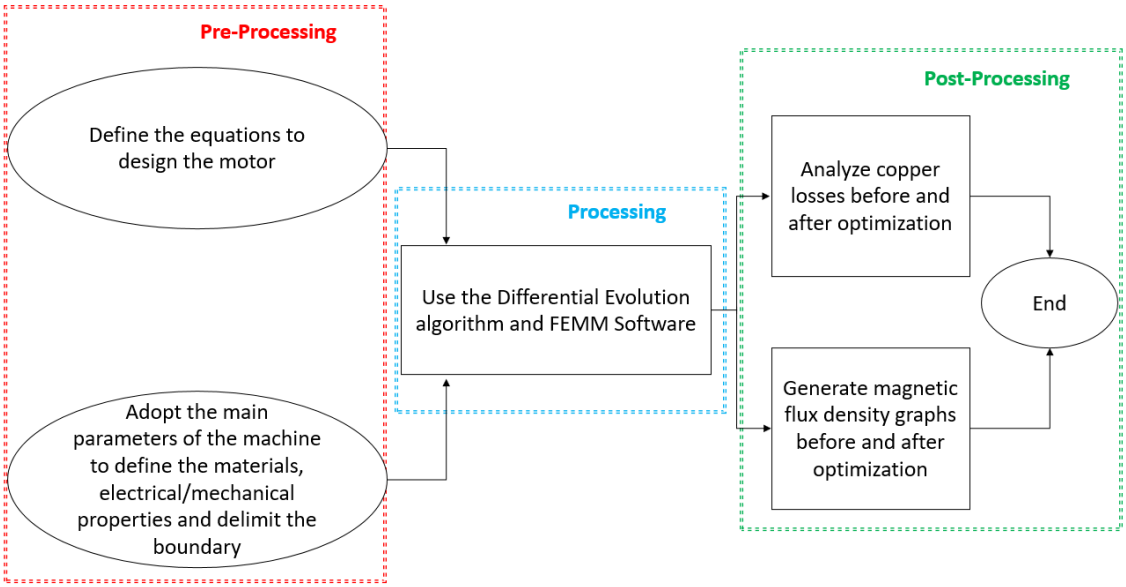

Fig. 6. Flowchart of case study steps to minimize VRM copper losses.

TABLE I. ELECTRICAL CHARACTERISTICS OF THE SINGLE-PHASE VARIABLE RELUCTANCE MOTOR

Parameters	Values	Parameters	Values
k1	1.44	η	0.80
TRV	16000	Nr	6
P	5,516.25 W	Bsat	1.85 T
RPM	1760 rpm	μ_0	$4\pi.10^{-7}$ H/m
Ns	6	Ip	31.34 A
V	220 V	Jc	6.0 A/mm^2

TABLE II. SINGLE-PHASE VARIABLE RELUCTANCE MOTOR DIMENSIONS BEFORE OPTIMIZATION

Parameters	Values	Parameters	Values
βs	30 °	hs	31.20 mm
βr	30.72 °	hr	17.50 mm
Dr	134.60 mm	ts	35.00 mm
Ds	236.04 mm	tr	35.65 mm
L	193.20 mm	ac	3.31 mm^2
Ys	19.205 mm	g	0.32 mm
Yr	21.40 mm	NE	20 turns

Thus, the formulation of the objective function of the problem is a single objective function with the intent to satisfy the adopted optimization criteria. In (26) it is possible to verify the objective function, that is, minimization of copper losses.

$$f = \frac{\rho_0 lm Ns}{ac} I_{rms}^2 \tag{26}$$

Where I_{rms} is the rms current; ρ_0 is the copper resistivity (1.72x10^{-8} Ω.m); lm is the conductor average length. Therefore, the limits of the variables must be respected, as shown from (27) to (31).

ISSN 2179-1074

$$120 < Dr < 140 \tag{27}$$

$$16 < Ys < 22 \tag{28}$$

$$18 < Yr < 24 \tag{29}$$

$$30 < Deix < 60 \tag{30}$$

$$0.30 < g < 0.60 \tag{31}$$

Thus, the VRM can be modeled, making it possible to simulate the project through the FEMM software.

B. Maximization of Flux Linkage in 8/6 VRM

In this case study, the flux linkage of one of the phases of the 8/6 VRM will be calculated by the software ONELAB through a magnetostatic analysis, under fixed values of excitation current. Unlike the methodology presented in Fig. 6, specifically in the pre-processing stage, the geometric parameters will be modified with the exception of βs, βr, Ds, L, ac, NE in order to keep the electrical characteristics and dimensions equivalent to the housing. The shaft diameter will also be changed in order to verify its effect on the magnetic flux calculation.

Aiming at maximizing the flux linkage per volumetric unit of magnetic material, the PSO algorithm will be applied in the same instance of the simulation interface. The search for a greater value of flux linkage leads to a greater capacity to produce torque for the same current density, since the volume is minimized in order to reduce the amount of magnetic material needed to build the VRM. As the magnetic flux and the core volume are two inversely proportional quantities for the same operating point of the VRM, the multi-objective algorithm SMPSO based on the PSO strategy will be applied. Through the Pareto front with non-dominated solutions, the optimal points can be chosen. Besides, the flux linkage per volumetric unit can be defined as an objective function in order to be maximized by a single-objective optimizer without caring to multiple functions trade-off. For comparative purposes, the DE algorithm will be used to search the global optimum. Electrical specifications and motor dimensions are shown in Table III and Table IV.

TABLE III. ELECTRICAL CHARACTERISTICS OF REFERENCE 8/6 VRM

Parameters	**Values**	**Parameters**	**Values**
k1	-	η	-
TRV	-	Nr	6
P	2200 W	Bsat	1.69 T
RPM	3500 rpm	μ_0	$4\pi.10^{-7}$ H/m
Ns	8	Ip	10 A
V	220 V	Jc	3.60 A/mm^2

The stator and rotor parts are composed of E185 Aperam 0.50 mm non-oriented silicon steel sheets, whose stacking factor is 97%, while the shaft is composed of 1020 carbon steel and has a $Deix$ dimension = 34.5 mm.

ISSN 2179-1074

TABLE IV. DIMENSIONS OF REFERENCE 8/6 VRM

Parameters	**Values**	**Parameters**	**Values**
βs	22.5 °	hs	22.0 mm
βr	24.5 °	hr	15.0 mm
Dr	90.5 mm	ts	17.8 mm
Ds	160.0 mm	tr	18.3 mm
L	63.0 mm	ac	2.08 mm^2
Ys	12.45 mm	g	0.30 mm
Yr	13.0 mm	NE	55 turns

For the SMPSO algorithm, two objective functions that characterize the multi-objective optimization problem were defined. The objective function f_1 is related to maximizing the magnetic flux linked in the coil,

$$f_1 = max\left(2\int_s \frac{L\,NEAz}{ab}ds\right) \tag{32}$$

Where L is the stack length, Az is the axial component of the magnetic vector potential $\vec{A}$ and ab is the cross-sectional area of the coil. The objective function f_2 minimizes the magnetic volume of the 8/6 VRM,

$$f_2 = min(Vol_{stator} + Vol_{rotor} + Vol_{shaft}) \tag{33}$$

Where Vol_{stator} is the stator volume, Vol_{rotor} is the rotor volume and Vol_{shaft} is the shaft volume. The search domain for the set of five upper and lower bounded geometric variables are defined,

$$80.5 < Dr < 100.5 \tag{34}$$

$$7.45 < Ys < 20.45 \tag{35}$$

$$10 < Yr < 18 \tag{36}$$

$$24.5 < Deix < 34.5 \tag{37}$$

$$0.30 < g < 0.60 \tag{38}$$

For the DE algorithm, a single-objective function, f_3, that characterize a single-objective optimization problem, is related to maximizing the ratio of the magnetic flux linked in the coil over the magnetic volume,

$$f_3 = max\left(\frac{2\int_s \frac{L\,NEAz}{ab}ds}{Vol_{stator} + Vol_{rotor} + Vol_{shaft}}\right) \tag{39}$$

The same bounds defined for SMPSO, (34)-(38), are also applied to DE algorithm.

VI. RESULTS AND DISCUSSION

Two case studies are investigated: the first one aims to optimize the geometry and electrical characteristics of windings of a single-phase VRM 6/6, minimizing copper losses; the second aims to optimize

received 12 Mar 2022; for review 20 Mar 2022; accepted 2 July 2022

ISSN 2179-1074

a restricted set of geometric parameters of a 4-phase VRM 8/6, maximizing the flux linkage in the phase coils per unit volume of magnetic core. In this way, by using the FEM, the results from DE and PSO algorithms will be compared and highlighted. Then, the magnetic flux densities of the motors are analyzed before and after the optimization.

A. Minimization of Copper Losses Using Finite Elements

The Differential Evolution algorithm was executed on MATLAB's environment with the following parameters: population size = 50, crossover probability = 0.8, rate of perturbation = 0.8, number of iterations = 50. In addition, the classic DE version was chosen among four versions of DE, which differ only in how new solutions are generated. The DE/rand/1/bin variation has proven to be slower, but more robust than the two methods that relied on the best-so-far vector. The Table V shows the obtained results from the optimized motor found after running the algorithm 10 times.

TABLE V. DIMENSIONS OF THE SINGLE-PHASE VRM AFTER DE OPTIMIZATION.

Parameters	**Values**	**Parameters**	**Values**
βs	30 °	hs	27.30 mm
βr	30.74 °	hr	15.60 mm
Dr	120 mm	ts	31.20 mm
Ds	210.50 mm	tr	31.80 mm
L	174.24 mm	ac	3.31 mm^2
Ys	17.65 mm	g	0.30 mm
Yr	23.25 mm	NE	18 turns

The Particle Swarm Optimization algorithm was executed on MATLAB's environment with the following parameters: population size = 50, inertia weight = 1, inertia weight damping ratio = 0.99, personal learning coefficient = 1.5 and global learning coefficient = 2.0. The Table VI shows the obtained results from the optimized motor found after running the algorithm 10 times.

TABLE VI. DIMENSIONS OF THE SINGLE-PHASE VRM AFTER PSO OPTIMIZATION.

Parameters	**Values**	**Parameters**	**Values**
βs	30 °	hs	25.50 mm
βr	30.74 °	hr	15.70 mm
Dr	120 mm	ts	31.20 mm
Ds	210.46 mm	tr	31.80 mm
L	172.40 mm	ac	3.31 mm^2
Ys	19.43 mm	g	0.30 mm
Yr	22.06 mm	NE	18 turns

Comparing the data between Table II, Table V and Table VI, the diameters, heights, widths, airgap, stack length and number of turns were reduced in the optimum model. In contrast, the conductor cross-sectional area and the polar arc of the stator were not modified. In the DE algorithm, there was an increase in the polar arc of the rotor and rotor yoke, and a decrease in the stator yoke. In the PSO algorithm, there was an increase in the polar arc of the rotor, and in the stator and rotor yoke.

The magnetic flux density at airgap in the original and optimized motors are shown in Fig. 7, Fig. 8 and Fig. 9 for two levels of excitation current, 31.34 A and 47.00 A.

received 12 Mar 2022; for review 20 Mar 2022; accepted 2 July 2022

ISSN 2179-1074

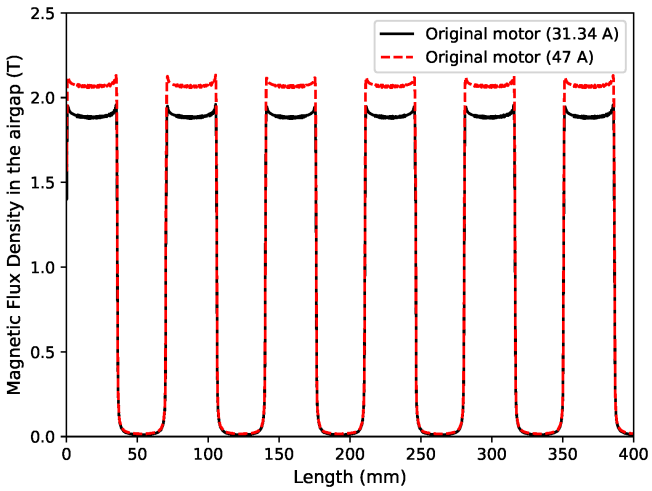

Fig. 7. Magnetic flux density at airgap before optimization.

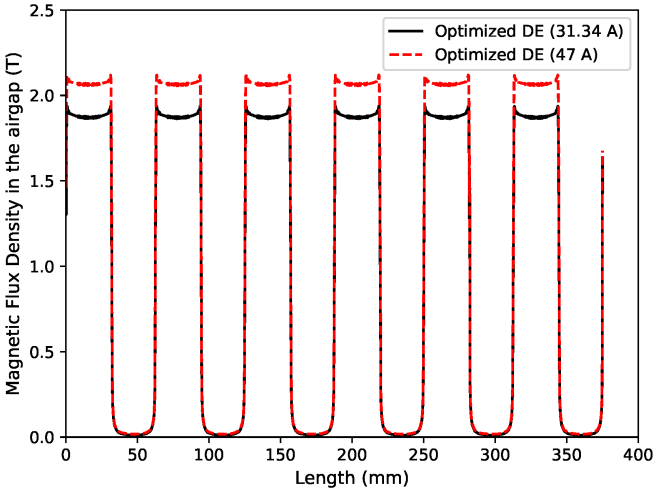

Fig. 8. Magnetic flux density at airgap after DE optimization.

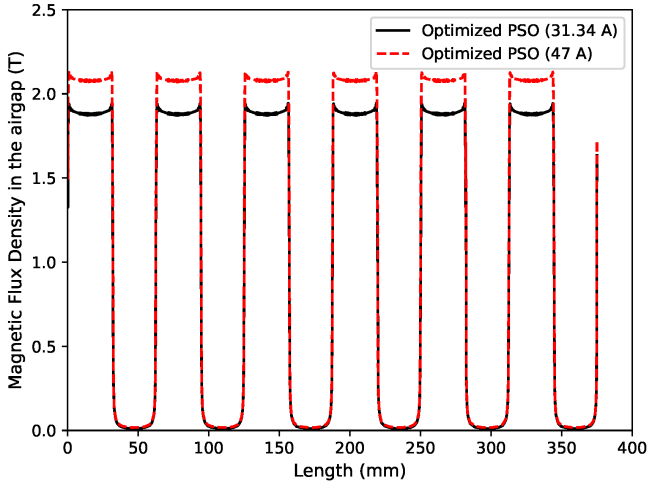

Fig. 9. Magnetic flux density at airgap after PSO optimization.

ISSN 2179-1074

At steady state regime, the magnetic flux densities at airgap under 31.34 A were reduced by using DE and PSO algorithms, 1.06% and 0.53%, respectively. It is worth mentioning that the flux density in the original motor was 1.88 T, while in the optimum ones using DE and PSO algorithms is 1.86 T and 1.87 T, respectively. Hence, the flux density remained close to the saturation level of the material.

Table VII shows copper losses for the two excitation currents before and after optimization, through the FEMM simulation and analytical calculation. The optimum motors produced by the optimizers have the copper losses and the magnetic flux densities at airgap reduced at two levels of excitation current. Therefore, the effectiveness of algorithms is presented.

TABLE VII. COPPER LOSSES BEFORE AND AFTER OPTIMIZATION.

Current (A)	**FEMM (W)**	**Analytical (W)**	**Difference (%)**
		Original	
31.34	118.68	119.92	1.034
47.00	266.98	269.80	1.045
		DE	
31.34	96.33	94.75	1.668
47.00	216.70	213.15	1.665
		PSO	
31.34	95.32	94.75	0.602
47.00	214.42	213.15	0.596

Furthermore, all the differences between the simulation and analytical computations are less than 1.668% in both scenarios. Highlighting the losses in copper in the simulation after optimization, there was a reduction of 18.83% and 19.68%, respectively for DE and PSO, in relation to the result presented in Table VII at 31.34 A in FEMM. While, in the analytical calculation after optimization, there was a reduction of 20.98% in both algorithms in relation to the result before optimization. We can conclude that the use of the adopted method for the computational simulations in this case study is of utmost importance for industry before the construction of the motor.

Fig. 10, Fig. 11 and Fig. 12 show the density of the magnetic flux in the motor at 31.34 A before and after the optimizations. Analyzing the results, it is noted that the algorithm with the best performance was the PSO for 6-pole machine. It is worth noting that both algorithms are effective with the results but the PSO algorithm stood out for the speed in convergence and showed better results. For electrical machine designers, it is worth noting that algorithms are simple to implement and should be validated using a computational tool with finite elements in addition to laboratory testing.

received 12 Mar 2022; for review 20 Mar 2022; accepted 2 July 2022

ISSN 2179-1074

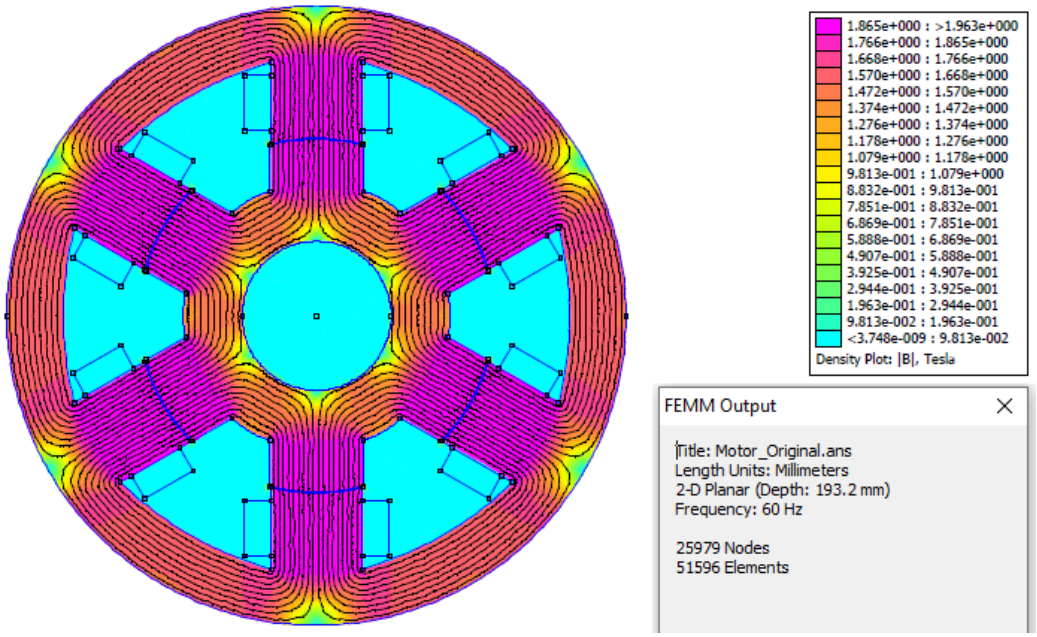

Fig. 10. Magnetic flux density in motor at 31.34 A before optimization.

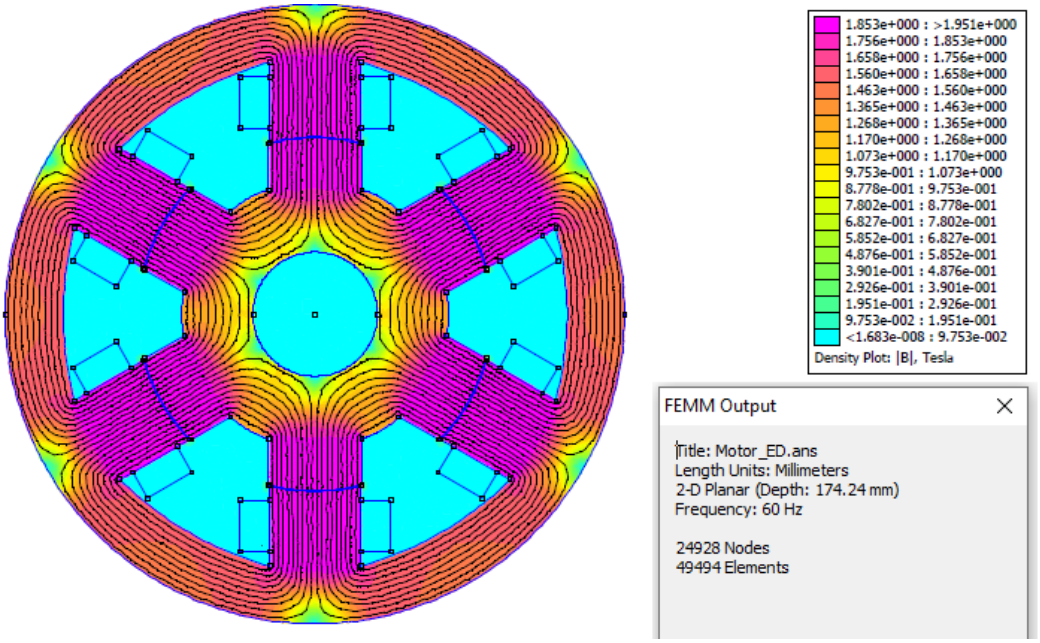

Fig. 11. Magnetic flux density in motor at 31.34 A after DE optimization.

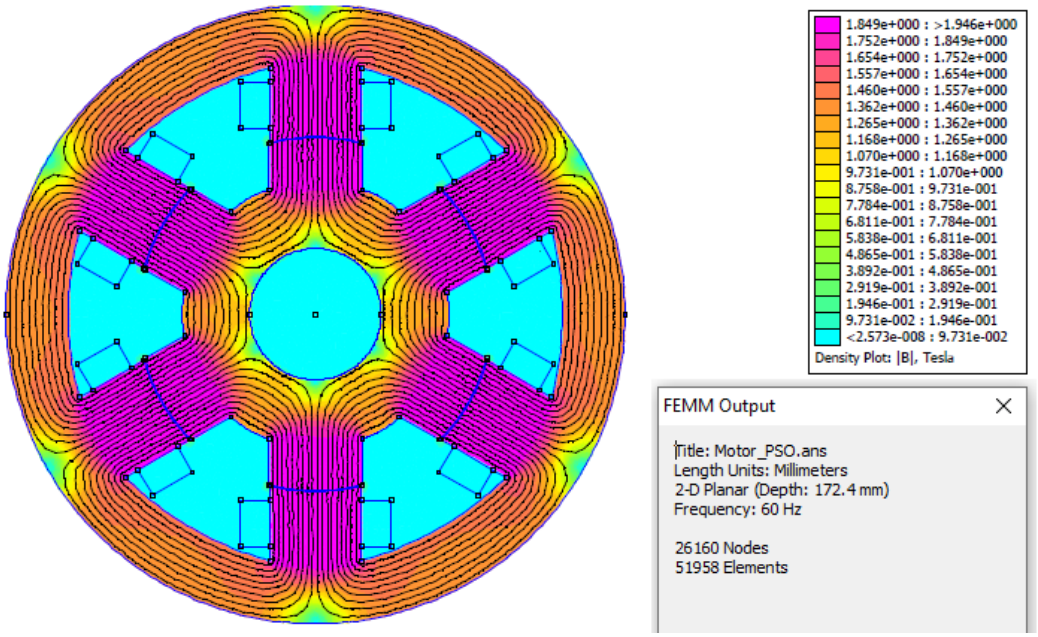

Fig. 12. Magnetic flux density in motor at 31.34 A after PSO optimization.

B. Maximizing the Flux Linkage through the ONELAB

The multi-objective SMPSO algorithm is executed on the interface of the ONELAB through a Python module call, available in the software package, by using the following parameters: swarm size = 100, leader size = 100, mutation probability = 0.1, mutation perturbation = 0.5, number of generations = 1000, $r_1 = r_2 = [0, 1]$, $C_1 = C_2 = [1.5, 2.5]$ and $w = [0.1, 0.5]$. The ranged parameters are randomly selected by the algorithm during the optimization, whilst mutation probability and mutation perturbation are not provided as control parameters, but presented herein only for information purpose.

Under the 10 A of constant rated current excitation and considering the phase at aligned position, the optimized results related to the non-dominated solutions are plotted in the Pareto front, as shown in Fig. 13.

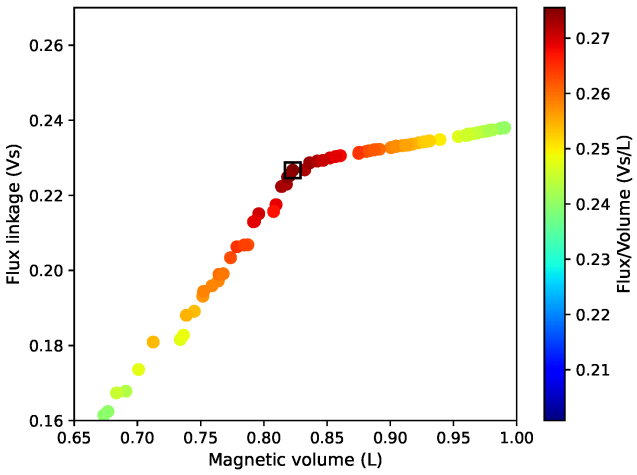

Fig. 13. Pareto front obtained from the multi-objective optimization through SMPSO algorithm.

The flux linkage (objective function f_1) tends to increase as the ferromagnetic volume (objective function f_2) increases. However, as from the solution which produces a magnetic volume of 0.82 L,

ISSN 2179-1074

indicated by the square marker at the center of figure, the rate of increase of the flux density by core volume is lower. For denoting this rate at each solution of Pareto front, a color bar was placed at the right side of the figure. The higher values indicate better exploitation of the magnetic flux density at a lower cost of core material. Therefore, the solution related to the square marker is the choice for the best optimized solution for carrying out post-processing simulations. Fig. 14 and Fig. 15 show the magnetic flux density in the reference and the best optimized 8/6 VRM, respectively, by feeding only one phase under 10 A.

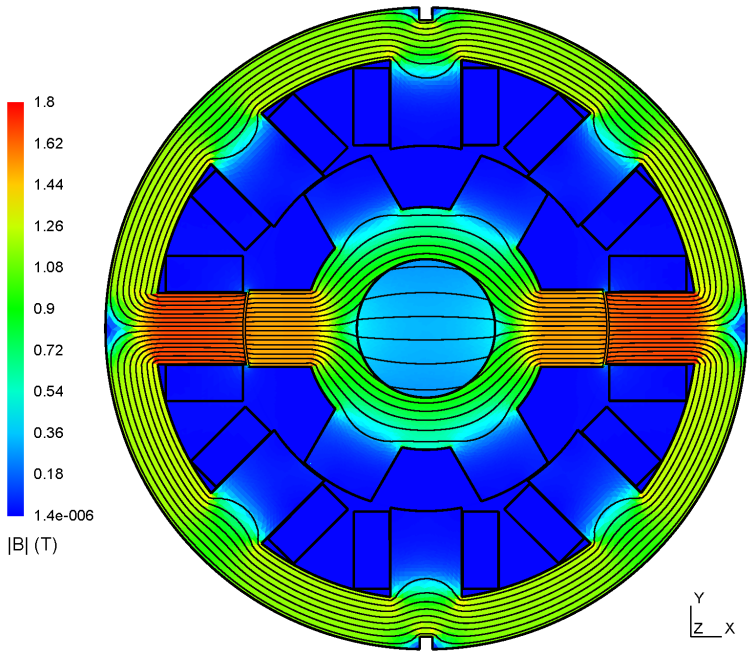

Fig. 14. Magnetic flux density in the reference 8/6 VRM.

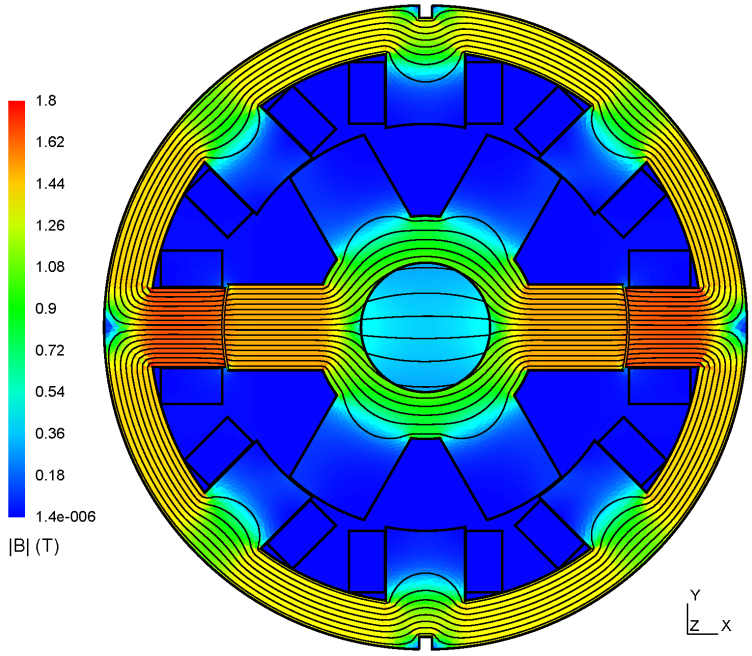

Fig. 15. Magnetic flux density in the 8/6 VRM optimized through SMPSO.

ISSN 2179-1074

In contrast, the single-objective DE algorithm is executed with classic DE version in the same manner as SMPSO algorithm, but using two different sets of parameters in order to find which combination is better suited to the given problem. The following set is defined: population size = 50, crossover probability = 0.45, rate of perturbation = 0.25 and number of iterations = 50. The second set only differs from the former in mutation and crossover operations: crossover probability = 0.9 and rate of perturbation = [0.5, 1.0]. Besides, a technique called dither that improves convergence behavior is applied to the latter. The rate of perturbation, F, is selected from the interval (0.5, 1.0) randomly for each difference vector. Higher values of the crossover probability, CR, is more appropriate when parameter dependence is encountered, which frequently occurs in real-world optimization problems.

At the same motor simulating conditions defined for carrying out the SMPSO optimization, the convergence of the DE algorithm for the two sets of parameters is shown in Fig. 16.

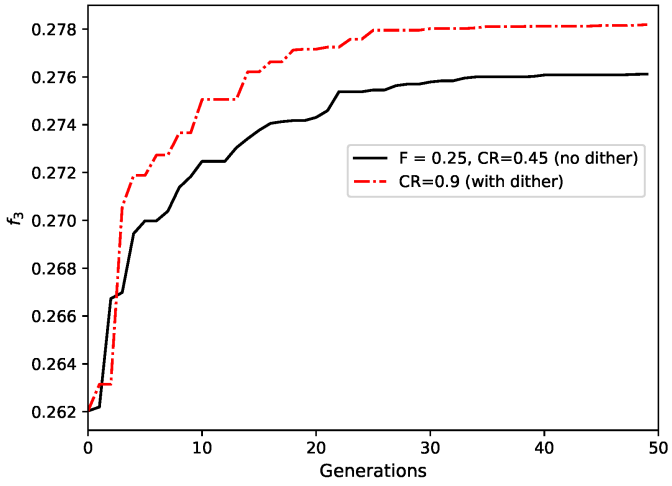

Fig. 16. Convergence of the DE algorithm.

The convergence results were obtained from the runs that achieved the highest values for the function f_3, after running the algorithm 10 times. One notes that higher values of F and CR benefits the search of global optimum for the given problem, as the dither method employs values for F bigger than 0.5. However, a solid conclusion cannot be drawn from convergence speed, since both curves do not converge to each other. Moreover, the maximum values of the function f_3 found for the first and second parameter sets were 0.2761 and 0.2781, respectively, whereas the maximum value of the corresponding rate (flux/volume) found by the multi-objective SMPSO algorithm was 0.2755.

Choosing the solution from DE run with dither technique, the magnetic flux density was calculated in the optimized 8/6 VRM, as shown in Fig. 17.

ISSN 2179-1074

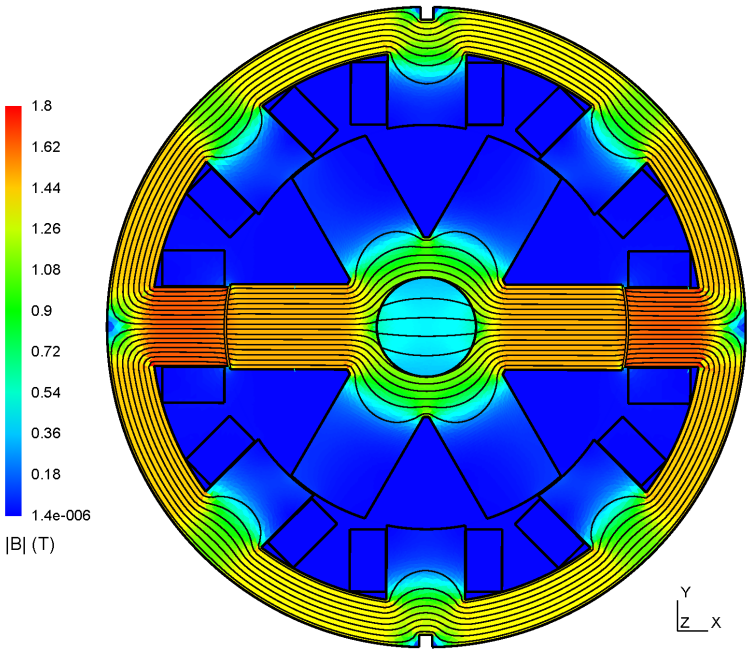

Fig. 17. Magnetic flux density in the 8/6 VRM optimized through DE (CR=0.9 with dither).

Table VIII and Table IX show the optimum variables (bounded and changed variables) according to the best optimized motor through SMPSO and DE algorithms, respectively.

TABLE VIII. DIMENSIONS OF 8/6 VRM AFTER SMPSO OPTIMIZATION

Parameters	**Values (mm)**	**Parameters**	**Values (mm)**
g	0.3	hs	18.05
Dr	100.5	hr	22.51
Ys	11.39	ts	19.72
Yr	11.66	tr	21.32
Deix	32.151	-	-

TABLE IX. DIMENSIONS OF 8/6 VRM AFTER DE OPTIMIZATION

Parameters	**Values (mm)**	**Parameters**	**Values (mm)**
g	0.3	hs	18.34
Dr	100.5	hr	27.76
Ys	11.12	ts	19.72
Yr	10.04	tr	21.32
Deix	24.86	-	-

By simulating reference and optimized motors, the phase flux linkage and the flux density at a central point on yoke stator at 10 A and 15 A were obtained. The data are presented in Table X. At 10 A, the value of the flux linkage per unit volume ($Fc/Vmag$) increased 10% and 11.3%, whereas at 15 A, the factor increased 8.15% and 9.6% after SMPSO and DE optimization, respectively. The motor related to DE solution achieved the lowest volume, $Vmag$, and the biggest flux density value on yoke stator, BYs, with an increase of 20% for the latter, when compared against the reference model.

TABLE X. FLUX LINKAGE, MAGNETIC VOLUME AND FLUX DENSITY FOR THE THREE 8/6 VRM MODELS

Parameters	Values at 10 A	Values at 15 A
Reference		
Fc (Vs)	0.2065	0.2257
Vmag (L)	0.8251	0.8251
Fc/Vmag (Vs/L)	0.2503	0.2735
BYs (T)	1.198	1.3110
SMPSO		
Fc (Vs)	0.2267	0.2474
Vmag (L)	0.8228	0.8228
Fc/Vmag (Vs/L)	0.2755	0.2958
BYs (T)	1.434	1.519
DE		
Fc (Vs)	0.2253	0.2428
Vmag (L)	0.8101	0.8101
Fc/Vmag (Vs/L)	0.2786	0.2997
BYs (T)	1.461	1.571

Comparing the data from Table IV, VIII and IX, there was a 17% decrease in the stator pole height, hs, and a 10.8% increase in the stator pole width, ts. As the stator region experiments higher flux densities than rotor, the increase in flux linkage, Fc, seems to be more sensitive to increases in the bore diameter and the pole widths.

In order to validate the statement that the increase in flux linkage implies an increase in torque production capability, the rotor was rotated by one stroke (60 mechanical degrees) as the static torque was calculated through ONELAB. The results are shown in Fig. 18.

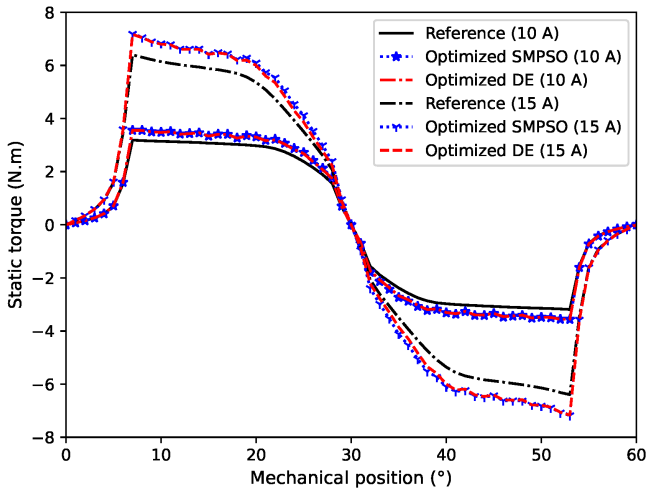

Fig. 18. Static torque obtained from de reference and optimized motors.

It could be observed in the torque waveforms that, both optimized motors produced equivalent torque values at two levels of current excitation for any rotor position. In addition, the peak torque achieved by the optimized models was 11.6% higher under 10 A, and 12.2% higher under 15 A than the reference motor. Thus, by changing only the VRM geometry dimensions it is possible to improve the torque production capability for the basic same volume of magnetic material.

The optimization problem was successfully solved by both DE and SMPSO algorithms. The increase in flux linkage and decrease in magnetic volume were achieved, simultaneously, by selecting: lower values for the stator and rotor yoke widths, and air gap length; higher values for the rotor diameter. However, the shaft diameter has had no impact in the optimization.

For this type of problem, defining higher values of F and CR (higher than 0.5) with the use of dither technique, the DE showed a better convergence through the search of global optimum after 50 generations for a population size = 50. Whereas, using standard parameters in the SMPSO, with a swarm size = 100, the algorithm showed, not only good results through a Pareto front, but found a close global optimum correlated to DE algorithm result, after 1000 generations. Since SMPSO is intended for constructing a Pareto front with the best possible non-dominated solutions, it is ideal for a designer who wants to make a trade-off between multiple functions, giving priority to performance at a minimal increase in cost material, for instance. Furthermore, the algorithms were useful to solve the problem, being capable to find reliable results at a reasonable speed.

VII. Conclusions

The DE and PSO algorithms were applied in two case studies: a single-phase 6/6 VRM, aiming the minimizing of copper losses; a 4-phase 8/6 VRM, aiming both the maximizing of the phase flux linkage and the minimizing of magnetic core volume. The classic DE (DE/rand/1/bin) version was chosen among the four variations due to its robustness. The single and 4-phase motors were modelled and simulated through the FE software FEMM and ONELAB, respectively.

In the first case study, after optimization procedures, most geometric parameters had a decrease in their values. The minimization of copper losses was satisfied by selecting higher values for the polar arc of the rotor and rotor yoke. Consequently, the DE and PSO algorithms were able to produce optimum motors achieving copper losses reduction of about 24% and a magnetic flux density reduction of 1% in the airgap at 31.34 A through FEMM. Moreover, comparing the copper losses obtained from simulation and analytical method, the computed differences for two current levels are lower than 1.7%. Therefore, the PSO algorithm was more effective. At the higher current excitation, the copper losses were also smaller.

In second case study, both algorithms were applied to the optimization problem. The SMPSO algorithm found a Pareto front with non-dominated solutions, where the increase in core volume implied the increase in flux linkage. The DE algorithm found a global optimum, correlated to the factor flux/volume, for two sets of parameters, in which the second set yielded better convergence. Moreover, the best optimized solution according to the factor flux/volume, found by SMPSO, aproached the global optimum found by DE. Both algorithms produced motors with bigger rotor poles, having a 17% decrease in the stator pole heights and a 10.8% increase in the stator pole widths. However, examining the factor flux/volume, it increased by 10% and 11.3% at 10 A, and 8.15% and 9.6% at 15 A through SMPSO and DE techniques, respectively, while the core volume was reduced from the latter. These changing in geometric parameters reflected in a higher torque production capability for both levels of current excitation. Therefore, for solving this type of optimization problems, designers should feel free to choose among both algorithms, paying attention to F and CR parameters.

Brazilian Microwave and Optoelectronics Society-SBMO *received 12 Mar 2022; for review 20 Mar 2022; accepted 2 July 2022*
Brazilian Society of Electromagnetism-SBMag *ISSN 2179-1074*

ACKNOWLEDGMENTS

Authors would like to thank CAPES (Ministry of Education Higher Education Personnel Improvement Coordination) for the resources allocated to the development of this research work.

REFERENCES

[1] J. Pyrhönen, T. Jokinen, and V. Hrabovcová, *Design of rotating electrical machines*. Chichester, U.K.: John Wiley & Sons, 2013.

[2] M. Balaji, V. Kamaraj, G. V. Suresh, K. S. B. K. Karunakar, N. V. Kumar, M. K. Yusof, A. A. Faisal, M. D. Sufian, S. Usop, I. G. C. Raj, *et al.*, "Differential evolution optimization combined with chaotic sequences for optimal design of switched reluctance machine," *Journal of Theoretical and Applied Information Technology (JATIT)*, vol. 27, no. 2, pp. 62–67, 2011.

[3] D. A. P. Correa, W. M. da Silva, S. I. Nabeta, and I. E. Chabu, "Control strategies applied for reducing the vibration and torque ripple of a special switched reluctance motor," *Journal of Microwaves, Optoelectronics and Electromagnetic Applications (JMOe)*, vol. 10, no. 1, pp. 203–216, 2011.

[4] A. C. F. Mamede, J. R. Camacho, and R. E. Araújo, "Influence of geometric dimensions on the performance of switched reluctance machine," *Machines*, vol. 7, no. 4, 2019. [Online]. Available: https://www.mdpi.com/2075-1702/7/4/71

[5] K. V. Price, R. M. Storn, and J. A. Lampinen, "The differential evolution algorithm," *Differential evolution: a practical approach to global optimization*, pp. 37–134, 2005.

[6] M. R. Sierra and C. A. Coello Coello, "Improving pso-based multi-objective optimization using crowding, mutation and-dominance," in *International conference on evolutionary multi-criterion optimization*, pp. 505–519, 2005.

[7] A. J. Nebro, J. J. Durillo, J. Garcia-Nieto, C. A. C. Coello, F. Luna, and E. Alba, "Smpso: A new pso-based metaheuristic for multi-objective optimization," in *2009 IEEE Symposium on computational intelligence in multi-criteria decision-making (MCDM)*, pp. 66–73, 2009.

[8] K. Rahman, B. Fahimi, G. Suresh, A. Rajarathnam, and M. Ehsani, "Advantages of switched reluctance motor applications to ev and hev: design and control issues," *IEEE Transactions on Industry Applications*, vol. 36, no. 1, pp. 111–121, 2000.

[9] J. D. Widmer, R. Martin, and M. Kimiabeigi, "Electric vehicle traction motors without rare earth magnets," *Sustainable Materials and Technologies*, vol. 3, pp. 7–13, 2015.

[10] A. C. F. Mamede, J. R. Camacho, and D. A. Andrade, "Design procedures and analysis for single-phase variable reluctance motors," *Renewable Energy and Power Quality Journal (RE&PQJ)*, vol. 1, pp. 216–221, 2016.

[11] H. Alharkan, S. Saadatmand, M. Ferdowsi, and P. Shamsi, "Optimal tracking current control of switched reluctance motor drives using reinforcement q-learning scheduling," *IEEE Access*, vol. 9, pp. 9926–9936, 2021.

[12] M. A. Patel, K. Asad, Z. Patel, M. Tiwari, P. Prajapati, H. Panchal, M. Suresh, R. Sangno, and M. Israr, "Design and optimisation of slotted stator tooth switched reluctance motor for torque enhancement for electric vehicle applications," *International Journal of Ambient Energy*, vol. 0, no. 0, pp. 1–6, 2021.

[13] T. J. E. Miller, *Switched Reluctance Motors and Their Control*. Oxford: Magna physics publishing and clarendon press, 1993.

[14] M. J. Moraes Filho, R. B. Bianchi, L. C. Gomes, D. A. Andrade, A. W. F. V. Silveira, J. A. Santos Jr, C. A. Oliveira, and W. G. Souza, "Projeto de máquina a relutância variável 8/6 e impacto do ângulo do polo do rotor em seu desempenho," in *XXI Congresso Brasileiro de Automática-CBA*, pp. 1644–1649, 2016.

[15] S. R. Kenneth and R. M. Storn, "Differential evolution-a simple and efficient heuristic for global optimization over continuous spaces," *Journal of Global Optimization*, vol. 11, no. 4, pp. 341–359, 1997.

[16] J. P. A. BASTOS, *Eletromagnetismo para engenharia: Estática e quase estática. rev*, Florianópolis: Ed. da UFSC, 2012.

[17] F. B. R. Mendes, J. V. Leite, N. J. Batistela, N. Sadowski, F. Suárez, and J. P. d. Barros, "Comparison and combination of techniques for determining the parameters of a magnetic hysteresis model," *Journal of Microwaves, Optoelectronics and Electromagnetic Applications*, vol. 18, pp. 408–426, 2019.

[18] C. A. C. Wengerkievicz, R. d. A. Elias, N. J. Batistela, N. Sadowski, P. Kuo-Peng, S. C. Lima, P. A. d. Silva, and A. Y. Beltrame, "Estimation of three-phase induction motor equivalent circuit parameters from manufacturer catalog data," *Journal of Microwaves, Optoelectronics and Electromagnetic Applications*, vol. 16, pp. 90–107, 2017.

received 12 Mar 2022; for review 20 Mar 2022; accepted 2 July 2022

ISSN 2179-1074